A Density Functional Study To Choose the Best Fluorophore for Photon-Induced Electron-Transfer (PET) Sensors

Abhijit Chatterjee,* Toshishige M. Suzuki, Yukiko Takahashi, and David A. Pacheco Tanaka[a]

Abstract: Anthracenes bearing aliphatic or aromatic amino substituents, which behave as molecular sensors, have shown their potential to act as photon-induced electron-transfer (PET) systems. In this PET, the fluorophore moieties are responsible for electron release during protonation and deprotonation. The principle of hard and soft acids and bases (HSAB) deals with both intra- and intermolecular electron migration. It is possible to calculate the localized properties in terms of Fukui functions in the realm of density functional theory (DFT) and thus calculate and establish a numerical matchmaking procedure that will generate an a priori rule for choosing the fluorophore in terms of its activity. We calculated the localized properties for neutral, anionic, and cationic systems to trace the course of the efficiency. A qualitative scale is proposed in terms of the feasibility of intramolecular hydrogen bonding. To investigate the effect of the environment of the nitrogen atom on protonation going from mono- to diprotonated systems, we calculated the partial density of states and compared the activity sequence with reactivity indices. The results show that location of the nitrogen atom in an aromatic ring does not influence the PET, but for aliphatic chains it plays a role. Furthermore, the protonation/deprotonation scenario has been explained. The results show that the reactivity indices can be used as a suitable property for scaling the activity of fluorophore molecules for the PET process.

Keywords: density functional calculations · donor–acceptor systems · electron transfer · reactivity indices · sensors

Introduction

Fluorescent signaling by the PET strategy is distinguished by its intrinsically supermolecular nature, since distinct components each perform one (or more) of the necessary functions.[1] A sensor molecule consists of three parts: A fluorophore module is the site for both photonic excitation and emission, a receptor module is responsible for guest complexation and decomplexation, and a spacer module holds the fluorophore and receptor close to, but separate from, each other. It is well known that life processes are usually successful only within a relatively narrow window of pH, and many other chemical species must also be held within narrow ranges of concentration. Organisms depend on such concentration windows for their survival.[2] It would be useful to rapidly screen microenvironments for the presence of such windows of pH. Fluorescent sensing is particularly capable of imaging concentrations of chemical species in microenvironments.[3–5] De Silva et al[6] proposed a predictive design for molecules with PET characteristics, which display strong fluorescence within a pH window. It involves self-assembly of ligands and metal moieties, especially transition metal cations. Ligands containing amino or pyridinyl groups and a fluorescent moiety display rich photophysical behavior in aqueous solution, due to variation in fluorescence intensity with pH. A ligand of the pyridine type quenches the fluorescence of a fluorophore like anthracene only when protonated,[6] while an amino group quenches the fluorescence of the same fluorophore only when not protonated.[7] This means that the fluorescence of aminomethylanthracenes is switched off as a result of PET.[8] Protonation of the amino group stops PET, and the fluorescence is switched on. Such proton-induced "off–on" switching is the normal logic of fluorescent PET sensors.[3] The opposite case of proton-induced "on–off" switching can achieved by using reversed-logic fluorescent PET sensors.[3] As this reaction is to be performed in aqueous medium it should be pH-dependent. If one knows the percentage of a particular species in a particular pH range it would be possible to switch advantageously from one species to another or from one architecture to another by simply tuning the pH or modulating the degree of protonation. Hence, if the fluorophore structure is known and the electron-donor/receptor property of the molecule can be tuned, then

[a] Dr. A. Chatterjee, T. M. Suzuki, Y. Takahashi, D. A. Pacheco Tanaka
Laboratory of Membrane Chemistry
National Institute of Advanced Industrial Science and Technology
AIST Tohoku
4-2-1 Nigatake, Miyagino-ku, Sendai 983-8551 (Japan)
Fax: (+81) 22-237-5217
E-mail: c-abhijit@aist.go.jp

DOI: 10.1002/chem.200204613

an active fluorophore suited for a particular PET sensing process can be proposed. This prompted us to use localized structure-based properties to obtain an activity scale for a range of molecules suitable for the PET process. So far there have been no such studies for rationalizing the phenomenon of PET for a set of molecules, for arranging them on an activity scale, and for understanding the mechanism of the process.

The principle of hard and soft acids and bases (HSAB) classifies the interaction between acids and bases in terms of global softness. Pearson proposed the global HSAB principle.[9] The global hardness was defined as the second derivative of the energy relative to the number of electrons at constant temperature and external potential, which includes the nuclear field. The global softness is the inverse of this. Pearson also suggested a principle of maximum hardness (PMH),[10] which states that, for a constant external potential, the system with the maximum global hardness is the most stable. This added a new dimension to understanding the driving forces of chemical processes. Recently, DFT has gained widespread use in quantum chemistry. Some DFT-based local properties, for example, Fukui functions and local softnesses,[11] have already been used to make reliable predictions for various types of electrophilic and nucleophilic reactions.[12–15] In our recent studies[16–18] we used a scale of reactivity indices for predicting intermolecular reactivity. Here, in the current study we deal with an intramolecular reactivity sequence to find the electrophilic and nucleophilic centers of a given molecule. We used the concept of relative nucleophilicity/electrophilicity proposed by Roy et al.[19] to choose the active site. They applied this concept to carbonyl compounds, and we also successfully used it to rationalize the adsorption of nitrogen heterocycles over smectites.[20]

In the present work we investigated some possible candidates as multidentate polytopic N donor ligands of the pyridine and amine types. We considered all feasible locations of the nitrogen atoms in both cases, and investigated the case with a phenyl ring to determine the electronic structure in the absence of nitrogen donors. The geometry of the optimized structures was studied to see if there is any influence of the location of the active centers on the performance of the molecule. The cases with and without protonation were studied to rationalize the "off–on" mechanism of the sensors during protonation. We could successfully grade the range of molecules studied in terms of their activity as fluorophores. Partial density of state (PDOS) calculations were performed with a special emphasis on the nitrogen centers, and the results are discussed in terms of the contribution of the respective atomic orbital to the respective molecular orbital. This methodology was used to find the best fluorophore from the range of available molecules.

Theory

In density functional theory, hardness η is defined by Equation (1)[21], where E is the total energy, N the number of electrons of the chemical species, and μ the chemical potential.

$$\eta = (\delta^2 E/\delta N^2)v(r)/2 = (\delta\mu/\mathrm{d}N)_v/2 \quad (1)$$

The global softness S is defined as the inverse of the global hardness η [Eq. (2)].

$$S = 1/2\,\eta = (\delta N/\delta\mu)_v \quad (2)$$

By using the finite-difference approximation, S can be approximated as Equation (3), where IE and EA are the first ionization energy and electron affinity of the molecule, respectively.

$$S = 1/(\mathrm{IE} - \mathrm{EA}) \quad (3)$$

The Fukui function $f(r)$ is defined by Equation (4)[11] where N is the total number of electrons, μ is the chemical potential, and v is the potential acting on an electron due to all nuclei present.

$$f(r) = [\delta\mu/\mathrm{d}v(r)]_N = [\delta\rho(r)/\delta N]_v \quad (4)$$

The function f is thus a local quantity which has different values at different points in the molecule. Since $\rho(r)$ as a function of N has slope discontinuities, Equation (1) provides three reaction indices [Eqs. (5a–c)][11].

$$f^-(r) = [\delta\rho(r)/\delta N]_v^- \quad \text{(for electrophilic attack)} \quad (5a)$$

$$f^+(r) = [\delta\rho(r)/\delta N]_v^+ \quad \text{(for nucleophilic attack)} \quad (5b)$$

$$f^0(r)[f^+(r) + f^-(r)]/2 \quad \text{(for radical attack)} \quad (5c)$$

In a finite-difference approximation, the condensed Fukui function[22] of an atom, say x, in a molecule with N electrons are defined as Equations (6a–c), where q_x is the electronic population of atom x in a molecule.

$$f_x^+ = [q_x(N+1) - q_x(N)] \quad \text{(for nucleophilic attack)} \quad (6a)$$

$$f_x^- = [q_x(N) - q_x(N-1)] \quad \text{(for electrophilic attack)} \quad (6b)$$

$$f_x^0 = [q_x(N+1) - q_x(N-1)]/2 \quad \text{(for radical attack)} \quad (6c)$$

The local softness $s(r)$ can be defined as Equation (7).

$$s(r) = (\delta\rho(r)/\delta\mu)_v \quad (7)$$

Equation (3) can also be written as Equation (8).

$$s(\mathrm{r}) = [\delta\rho(r)/\delta N]_v[\delta N/\delta\mu]_v = f(r)S \quad (8)$$

Thus, the local softness contains the same information as the Fukui function $f(r)$ plus additional information on the total molecular softness, which is related to the global reactivity with respect to a reaction partner, as stated in the HSAB principle. Atomic softness values can easily be calculated by using Equation (4) [Eqs. (9a–c)].

$$s_x^+ = [q_x(N+1) - q_x(N)]S \quad (9a)$$

$$s_x^- = [q_x(N) - q_x(N-1)]S \quad (9b)$$

$$s_x^0 = S[q_x(N+1) - q_x(N-1)]/2 \quad (9c)$$

Methods of Calculation

All calculations were carried out with DFT[23] by using the DMOL3 code of MSI Inc. A gradient-corrected BLYP functional[24, 25] and DNP basis set[26] was used throughout. Geometries of the interacting molecules 9-*N*-(2-phenylmethyl)aminomethylanthracene, 9-*N*-(2-pyridylmethyl)aminomethylanthracene, 9-*N*-(3-pyridylmethyl)aminomethylanthracene, 9-*N*-(4-pyridylmethyl)aminomethylanthracene, 9-*N*-(2-aminoethyl)aminomethylanthracene, and 9-*N*-[2-(methylamino)ethyl]aminomethylanthracene were fully optimized for calculating the reactivity indices. The structures of the molecules are shown in Figures 1 – 6. Single-point calculations on the cation and anion of each molecule at the optimized geometry of the neutral molecule were also carried out to evaluate Fukui functions and global and local softness. The condensed Fukui function and atomic softness were evaluated by using Equations (6) and (9), respectively. The gross atomic charges were evaluated by using the technique of electrostatic potential (ESP) driven charges. The methodology for the PDOS calculation is mentioned in the relevant section.

Results and Discussion

The aim of the current study is to choose the best fluorophore from a range of available molecules to act as a PET system mimicking the process in the microorganism. This was carried out in the following steps: 1) optimization of the molecules to determine the geometrical parameters, 2) calculation of the reactivity indices of the molecules to locate the active centers in the neutral nonprotonated molecules, 3) ordering of these molecules on a reactivity-index scale, 4) calculation of the HOMO – LUMO energy difference to predict the feasibility of electronic transition, and 5) comparing the activity of the nitrogen centers in the molecules in terms of their conformation, as predicted by PDOS.

Influence of geometric parameters on the properties of the molecules: The molecules studied are labeled as shown in Figure 1, Figure 2, Figure 3, Figure 4, Figure 5, and Figure 6.

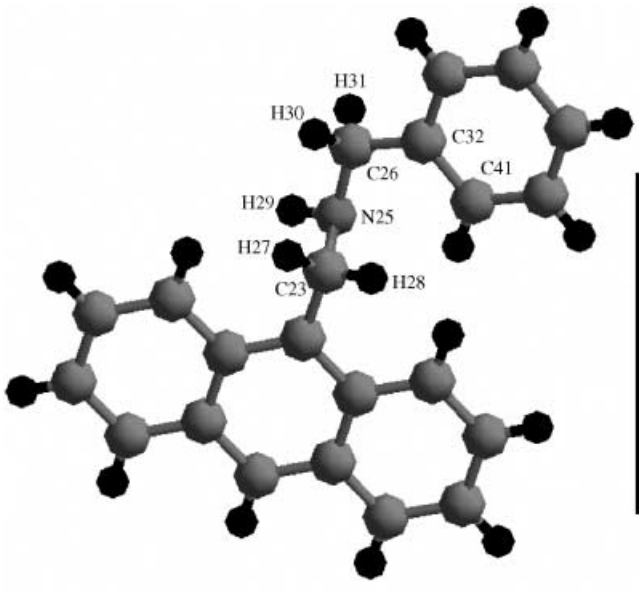

Figure 1. Optimized geometry of 9-*N*-(2-phenylmethyl)aminomethylanthracene with important atoms labeled.

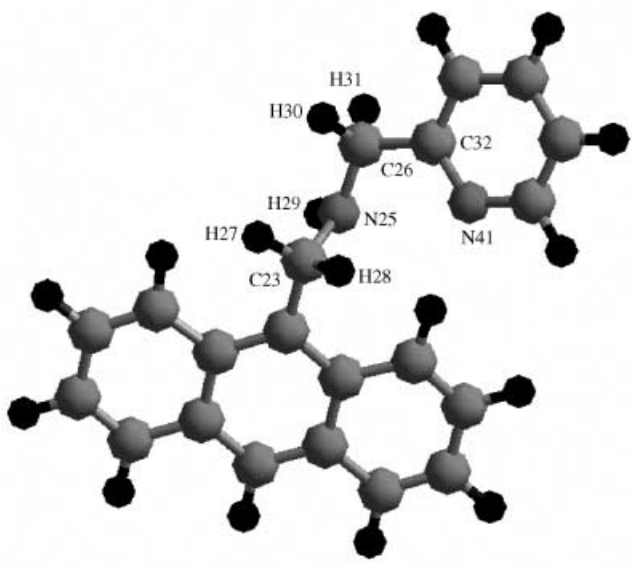

Figure 2. Optimized geometry of 9-*N*-(2-pyridylmethyl)aminomethylanthracene with important atoms labeled.

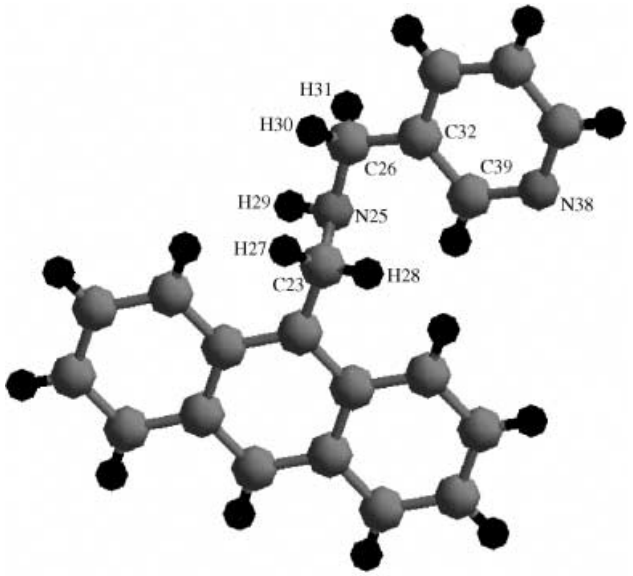

Figure 3. Optimized geometry of 9-*N*-(3-pyridylmethyl)aminomethylanthracene with important atoms labeled.

The molecules were fully optimized, and the geometric parameters, that is, bond lengths and bond angles for the selected atoms, are listed in Table 1 and Table 2, respectively, in all cases going from the nonprotonated to diprotonated via monoprotonated forms. We compared the bond lengths C23–N25, N25–C26, C26–C32, and C32–N_{Py}. We found that for the phenyl-substituted compound all three bonds lengthen on going from the nonprotonated to the monoprotonated molecule. The C26–C32 bond, the linkage between the methylene carbon atom and the benzene ring, is the least affected by protonation. For the pyridine series there is a remarkable change in the bond length associated with N25 after protonation; the distance increases in the order of 2-, 3-, and 4-pyridylanthracene molecules. The distance remains

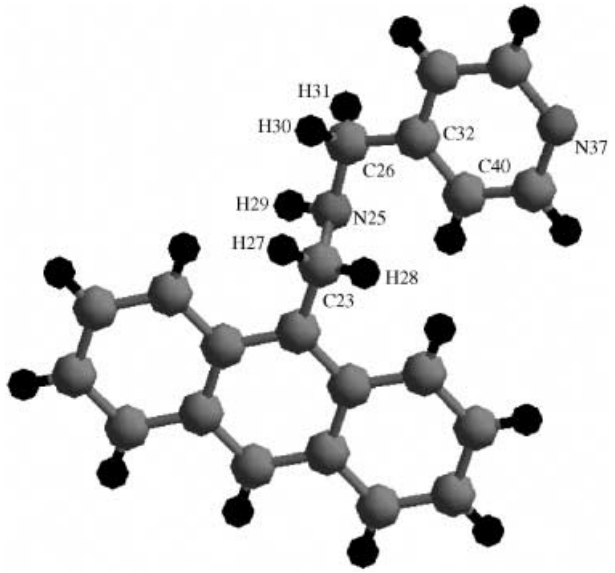

Figure 4. Optimized geometry of 9-*N*-(4-pyridylmethyl)aminomethylanthracene with important atoms labeled.

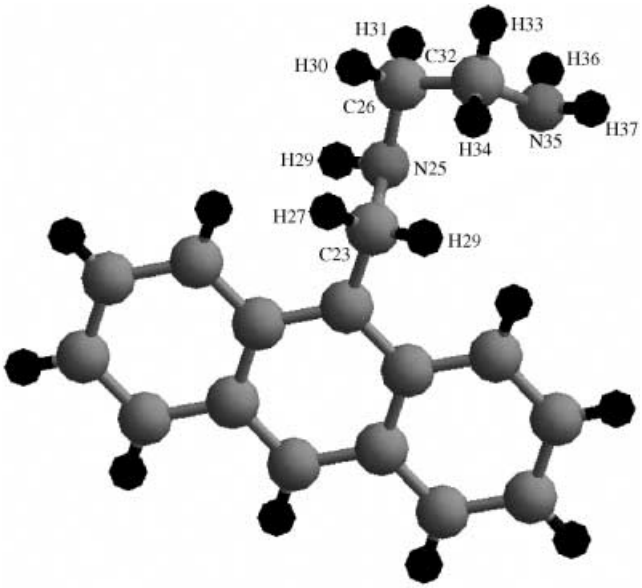

Figure 5. Optimized geometry of 9-*N*-(2-aminoethyl)aminomethylanthracene with important atoms labeled.

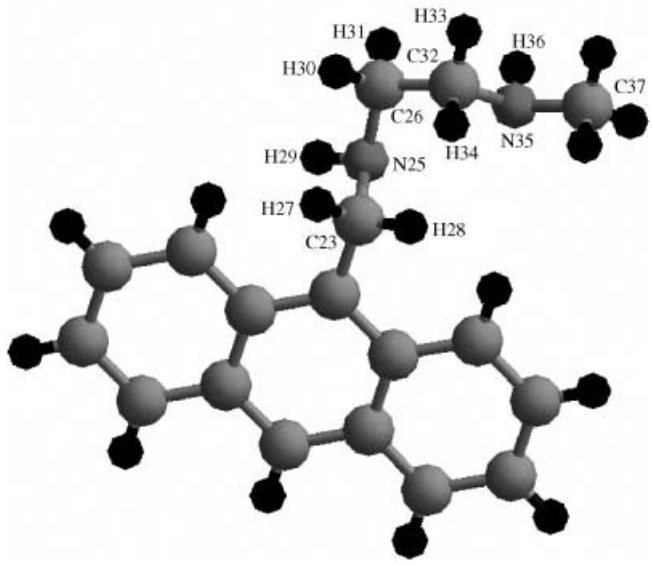

Figure 6. The optimized geometry of 9-*N*-[2-(methylamino)ethyl]aminomethylanthracene with important atoms labeled.

Table 1. Bond lengths for the molecules concerned before and after protonation.

Molecule[a]	Bond lengths [Å]				
	C23–N25	N25–C26	C26–C32	C32–N_{py}[c]	
2-phenyl-anth	a) 1.368	a) 1.342	a) 1.412	–	–
	b) 1.451	b) 1.433	b) 1.421	–	–
2-pyridyl-anth	a) 1.362	a) 1.341	a) 1.428	a) 1.259 (N41)	
	b) 1.446	b) 1.424	b) 1.428	b) 1.260	–
	c) 1.446	c) 1.439	c) 1.437	c) 1.310	–
3-pyridyl-anth	a) 1.365	a) 1.345	a) 1.415	a) 2.229 (N38)[c]	
	b) 1.456	b) 1.435	b) 1.417	b) 2.235	–
	c) 1.458	c) 1.435	c) 1.419	c) 2.252	–
4-pyridyl-anth	a) 1.368	a) 1.342	a) 1.421	a) 2.574 (N37)[c]	
	b) 1.505	b) 1.482	b) 1.491	b) 2.578	–
	c) 1.522	c) 1.482	c) 1.490	c) 2.594	–
				C32–N35	N35–C37
$NH_2CH_2CH_2$-antha[d]	a) 1.371	a) 1.383	a) 1.394	a) 1.324	
	b) 1.448	b) 1.429	b) 1.406	b) 1.335	–
	c) 1.449	c) 1.436	c) 1.406	c) 1.404	–
$CH_3NHCH_2CH_2$-antha[d]	a) 1.364	a) 1.342	a) 1.407	a) 1.343	a) 1.329
	b) 1.446	b) 1.433	b) 1.406	b) 1.350	b) 1.331
	c) 1.450	c) 1.441	c) 1.410	c) 1.434	c) 1.403

[a] anth = methylaminomethylanthracene. [b] a = nonprotonated, b = monoprotonated, c = diprotonated. [c] Nonbonding distance between C32 and the nitrogen atom of the pyridine ring, except for 2-pyridyl. N_{py} = pyridyl nitrogen, numbers are given in parenthesis. [d] antha = aminomethylanthracene.

almost same for both the di- and monoprotonated forms for all three molecules. There is almost no change in the C26–C32 bond length for 2- and 3-pyridyl-containing molecules, even after protonation, whereas a change occurs in the 4-pyridyl-substituted molecule, in which the pyridyl nitrogen atom is *trans* to the methylene group. Except for the diprotonated form of the 4-pyridyl compound, this bond length remains same as in the monoprotonated molecule. We determined the distance between C32 and the nitrogen atom of the pyridine ring for the set of molecules. The distances are nonbonding for all molecules except for the 2-pyridyl compound. In the 2-pyridyl compound there is no change in this bond length on transition from the nonprotonated to the monoprotonated species, but the bond length increases on going to the diprotonated form. The same trend is observed for the two other cases, in spite of the nonbonding nature of this distance. We determined the bond length between C32–N35 for aminoalkyl-substituted aminoanthracenes. The trend is almost same as that observed in the case of aromatic ring for the C23–N25, N25–C26, and C26–C32 bond lengths. The bond length involving N35 increases remarkably for the diprotonated forms. In the compound with a terminal methyl group, the bond length increases steadily from the nonprotonated via the monoprotonated to the diprotonated form. With regard to the central nitrogen atom the trend is the same for both

Table 2. Bond angles for the molecules concerned before and after protonation.

Molecule[a]	Bond angles[b] [°]		
	C23-N25-C26	N25-C26-C32	C26-C32-C/N
2-phenyl-anth	a) 120.2	a) 116.1	a) 121.3 (C41)
	b) 116.6	b) 119.6	b) 124.3
2-pyridyl-anth	a) 120.1	a) 115.5	a) 119.3 (N41)
	b) 114.9	b) 116.4	b) 119.3
	c) 115.4	c) 116.6	c) 120.1
3-pyridyl-anth	a) 119.9	a) 115.8	a) 121.1 (C39)
	b) 116.1	b) 118.8	b) 125.4
	c) 116.2	c) 118.6	c) 124.2
4-pyridyl-anth	a) 120.1	a) 116.2	a) 121.2 (C40)
	b) 116.5	b) 119.5	b) 125.0
	c) 115.3	c) 120.1	c) 125.5
$NH_2CH_2CH_2$-antha[c]	a) 114.9	a) 112.7	a) 107.2 (N35)
	b) 115.7	b) 115.6	b) 114.7
	c) 115.7	c) 118.8	c) 118.3
$CH_3NHCH_2CH_2$-anth	a) 120.8	a) 115. 5	a) 113.1 (N35)
	b) 115.7	b) 116. 7	b) 113.3
	c) 115.3	c) 119.1	c) 116.3

[a] anth = methylaminomethylanthracene. [b] a = nonprotonated, b = monoprotonated, c = diprotonated. [c] antha = aminomethylanthracene.

pyridyl- and amino-substituted molecules, whereas the effect for the other nitrogen atoms is more pronounced for the amino-type compounds.

We measured the C23-N25-C26, N25-C26-C32, and C26-C32-C/N (depending on the atom present) bond angles of the molecules at their optimized geometries for all possible cases mentioned above. With phenyl substitution, C23-N25-C26 decreases and N25-C26-C32 increases on protonation. This means that the benzene ring moves away from the nitrogen atom. For the pyridyl-substituted molecules C23-N25-C26 decreases on protonation and remains almost unchanged on further protonation. The N25-C26-C32 angle increases on protonation but remains almost the same after diprotonation. The same trend is also found for C26-C32-C/N (the terminal atoms for the 2-, 3-, and 4-pyridyl compounds are N41, C39, and C40, respectively). After protonation, the pyridyl ring also moves away from the central nitrogen atom, irrespective of the position of the nitrogen atom in the pyridyl ring. For the aliphatic amino substituents the C23-N25-C26 angle increases on protonation and remains unchanged after the second protonation step. The N25-C26-C32 angle shows a similar incremental trend to that observed in the case of aromatic rings. The effect of the second protonation here is more pronounced than those of aromatic ring systems. A similar trend of increasing C26-C32-C/N with increasing degree of protonation is observed. The difference is more pronounced after the second protonation. Different contributions from aliphatic chains and aromatic rings are observed.

Activity of interacting fluorophore molecules in terms of reactivity index: The global softness values were calculated for each of the molecules (Table 3). It can be seen in Table 3 that no systematic ordering is evident for the global softness values of the ranges of molecules tested here. The values are higher for some compounds, and lower for others. Therefore, to test the HSAB principle, it is necessary to analyze the local softness values, Fukui functions, or reactivity indices for the constituent atoms of the interacting molecular species are more reliable parameters. The local electrophilicities s_x^+ and nucleophilicities s_x^- were calculated and are presented in Tables 4–9. These allow us to estimate the relative tendency of an atomic center to behave as an electrophile or a nucleophile. The local electrophilicity (s_x^+) and nucleophilicity (s_x^-) have been calculated and are presented in Tables 4–9. The results show that for intramolecular electrophilicity and nucleophilicity there are some anomalous cases in which a specific atom shows both high electrophilicity and nucleophilicity, and to rationalize this a concept of relative electrophilicity/nucleophilicity is more appropriate. Relative nucleophilicity is the nucleophilicity of a site relative to its own electrophilicity, and vice versa for relative electrophilicity. The relative nucleophilicity and electrophilicity also take care of the basis-set and correlation effects present in localized calculations. We calculated the reactivity indices for the nonprotonated moieties, and used the result to predict their activities towards protonation, or, in other words, we can estimate the probability of intramolecular hydrogen bonding. The coexistence of nucleophilic and electrophilic sites will result in intramolecular hydrogen bonding, whereby the center of highest relative nucleophilicity interacts with the center of highest relative electrophilicity. Depending on the activity of the respective centers the electron donor/acceptor property will vary. We calculated the relative nucleophilicities and electrophilicities for all the important constituent atoms of the molecules in this study. We neglected the anthracene part and part of the pyridyl or phenyl ring for the sake of clarity. The atoms of the molecules considered are labeled in Figures 1–6. As can be seen in Table 4 for 9-*N*-(phenyl-

Table 3. Global softness values [a.u.].

Molecule[a]	Global softness
2-phenyl-anth	3.68582
2-pyridyl-anth	3.69237
3-pyridyl-anth	3.63506
4-pyridyl-anth	3.62435
$NH_2CH_2CH_2$-antha[b]	2.34982
$CH_3NHCH_2CH_2$-antha[b]	2.69341

[a] anth = methylaminomethylanthracene. [b] antha = aminomethylanthracene.

Table 4. Condensed local softnesses for all constituent atoms except the anthracene ring and four carbon atoms of the benzene ring in 9-*N*-(phenylmethyl)aminomethylanthracene.

Atom	s_x^+	s_x^-	s_x^+/s_x^-	s_x^-/s_x^+
C23	0.121	0.258	0.468	2.132
H27	0.136	0.058	2.344	0.426
H28	0.110	0.070	1.571	0.636
N25	0.165	0.917	0.179	5.557
H29	0.254	0.342	0.742	1.346
C26	0.331	0.213	1.553	0.643
H30	0.184	0.033	5.575	0.179
H31	0.169	0.029	5.827	0.171
C32	0.088	0.136	0.647	1.545
C41	0.154	0.055	2.800	0.357

methyl)aminomethylanthracene C26 has the highest s_x^+ and N25 has the highest s_x^-, but the relative electrophilicity s_x^+/s_x^- is highest for H31, and the highest value of the relative nucleophilicity s_x^-/s_x^+ is that for N25. Hence, H31 is the most probable site of attack by a nucleophile, and N25 is favored for attack by an electrophile.

In the case of 9-*N*-(2-pyridylmethyl)aminomethylanthracene the highest local softness value for high electrophilicity is found for N25, and N41 shows the highest nucleophilicity (Table 5). However, when we calculated the relative electrophilicity we found that H29 has the highest value, that is, it will be attacked by a nucleophile. The highest relative nucleophilicity is exhibited by N41, which is thus the best candidate for attack by an electrophile. The same trend in relative electrophilicity/nucleophilicity is found for the other two pyridyl-substituted compounds, 9-*N*-(3-pyridylmethyl)aminomethylanthracene and 9-*N*-(4-pyridylmethyl)aminomethylanthracene. For both compounds the highest value of the relative electrophilicity is found for H29, and the highest value of the relative nucleophilicity for N38 and N37, respectively. The results are listed in Tables 6 and 7. Table 8 shows that for 9-*N*-(2-aminoethyl)aminomethylanthracene the highest electrophilicity is found for N35, and the highest nucleophilicity for H37. However, the relative electrophilicity shows the highest value for H29, and the highest value of the relative nucleophilicity is that for H37. This shows that H29 of the amine will be more susceptible to nucleophilic attack, while H37 will be susceptible to electrophilic attack. For 9-*N*-[2-(methylamino)ethyl]aminomethylanthracene the trend is the same for the relative electrophilicities, but different for the relative nucleophilicities, as can be seen in Table 9. Atom N35 shows the highest electrophilicity and nucleophilicity, which is ambiguous; however, in terms of relative nucleophilicity C23 has the highest value, but N35 still has the highest relative electrophilicity. This is may be due to the terminal methyl group, which is electron-withdrawing in nature. These results show that protonation is more favorable in pyridyl-type molecules and even phenyl-substituted molecules, but is less favorable for the compounds with aliphatic amino substituents. The situation is slightly improved for amines with a

Table 5. Condensed local softness for all the constituent atoms except the anthracene ring and the carbon atoms of the pyridine ring in 9-*N*-(2-pyridylmethyl)aminomethylanthracene.

Atom	s_x^+	s_x^-	s_x^+/s_x^-	s_x^-/s_x^+
C23	0.195	0.007	27.85	0.035
H27	0.107	0.007	15.28	0.065
H28	0.007	0.011	0.636	1.571
N25	0.893	0.070	12.75	0.078
H29	0.358	0.007	51.14	0.019
C26	0.232	0.011	21.09	0.047
H30	0.092	0.048	1.911	0.521
H31	0.022	0.295	0.074	13.41
C32	0.096	0.354	0.271	3.687
N41	0.022	1.085	0.020	49.31

Table 6. Condensed local softnesses for all the constituent atoms except the anthracene ring and carbon atoms of the pyridine ring in 9-*N*-(3-pyridylmethyl)aminomethylanthracene.

Atom	s_x^+	s_x^-	s_x^+/s_x^-	s_x^-/s_x^+
C23	0.065	0.025	2.600	0.384
H27	0.207	0.181	1.143	0.874
H28	0.116	0.359	0.323	3.094
N25	0.665	0.508	18.30	0.763
H29	1.283	0.023	54.02	0.017
C26	0.388	0.072	5.388	0.185
H30	0.537	0.101	5.316	0.188
H31	0.163	0.149	1.093	0.914
C32	0.258	1.806	0.142	7.000
N38	0.003	0.782	0.003	260.66

Table 7. Condensed local softnesses for all the constituent atoms except the anthracene ring and the carbon atoms of the pyridine ring in 9-*N*-(4-pyridylmethyl)aminomethylanthracene.

Atom	s_x^+	s_x^-	s_x^+/s_x^-	s_x^-/s_x^+
C23	0.250	0.047	5.319	0.188
H27	0.057	0.007	8.142	0.122
H28	0.065	0.004	16.25	0.061
N25	0.924	0.004	66.00	0.015
H29	0.329	0.004	82.25	0.012
C26	0.206	0.032	6.437	0.155
H30	0.036	0.010	3.600	0.277
H31	0.025	0.014	1.785	0.056
C32	0.144	0.123	1.170	0.854
N37	0.014	3.882	0.003	277.28

Table 8. Condensed local softnesses for all the constituent atoms except the anthracene ring in 9-*N*-(2-aminoethyl)aminomethylanthracene.

Atom	s_x^+	s_x^-	s_x^+/s_x^-	s_x^-/s_x^+
C23	0.401	0.408	0.982	1.017
H27	0.371	0.022	16.86	0.059
H28	0.244	0.024	10.16	0.098
N25	0.009	0.009	1.00	1.00
H29	0.594	0.024	24.75	0.040
C26	0.383	0.079	4.848	0.206
H30	0.298	0.022	13.54	0.073
H31	0.415	0.029	14.31	0.069
C32	0.462	0.148	3.121	0.320
H33	0.291	0.070	4.157	0.240
H34	0.270	0.028	9.642	0.103
N35	0.784	0.697	1.124	0.889
H36	0.364	0.206	1.766	0.565
H37	0.646	1.517	0.425	2.348

Table 9. Condensed local softnesses for all constituent atoms except the anthracene ring in 9-*N*-[2-(methylamino)ethyl]aminomethylanthracene.

Atom	s_x^+	s_x^-	s_x^+/s_x^-	s_x^-/s_x^+
C23	0.048	0.091	0.527	1.895
H27	0.158	0.191	0.827	1.208
H28	0.175	0.123	1.422	0.702
N25	0.379	0.083	4.566	0.218
H29	0.651	0.048	13.562	0.073
C26	0.603	0.169	3.568	0.280
H30	0.183	0.029	6.310	0.158
H31	0.239	0.226	1.057	0.945
C32	1.088	0.119	9.142	0.109
N35	2.566	0.503	5.101	0.196
H36	0.692	0.250	2.768	0.361
C37	1.090	0.331	3.293	0.303

terminal methyl group. The relative nucleophilicity/elctrophilicity studies show that the active centers of the molecule themselves are susceptible to electrophilic and nucleophilic attack. There is one electrophilic center and one nucleophilic center for each molecule, with different ranges of activity. It seems that mono-protonation is more favorable than diprotonation. It is also observed that for pyridyl substituents H29, bonded to N25, is electrophilic and the nitrogen atom in the pyridine ring is neucleophilic. Hence, in these cases there is the possibility of intramolecular hydrogen bonding between the pyridine nitrogen atom and another proton center present in the molecule, depending on its structure.

This finding supports the postulate of Amendala et al.,[27] who calculated the protonation constants for two sets of amine- and pyridine-type compounds. They showed that, irrespective of the ligand, the value for the second protonation is much higher than that of the first protonation step. They assumed that this might be due to the formation of an intramolecular hydrogen bond between the protonated amino group and the pyridine nitrogen atom in the the other half of the molecule.

Reactivity-index scale: The aim of the current study is to choose a molecule from an available variety of fluorophores suitable for PET process. The order of global softness for the fluorophore types is as follows: $NH_2CH_2CH_2$ – anthracene < $CH_3NHCH_2CH_2$ – anthracene < 4-pyridyl – anthracene < 3-pyridyl – anthracene < 2-phenyl – anthracene < 2-pyridyl – anthracene. In terms of relative electrophilicity of the atoms of the molecules the order for highest values is as follows: 4-pyridyl – anthracene > 3-pyridyl – anthracene > 2-pyridyl-anthracene > $NH_2CH_2CH_2$ – anthracene > $CH_3NHCH_2CH_2$ – anthracene > 2-phenyl – anthracene, while for as the relative nucleophilicities of the atoms of the molecules we found the following order of the highest values: 4-pyridyl – anthracene > 3-pyridyl – anthracene > 2-pyridyl – anthracene > 2-phenyl – anthracene > $NH_2CH_2CH_2$ – anthracene > $CH_3NHCH_2CH_2$ – anthracene. From the orders of activity it is clear that the location of the nitrogen atom does play a role in the PET process for these fluorophores. Since the trends of the relative electrophilicities and nucleophilicities are different, the contributions of the active sites residing in the receptor and in the flurophore must also differ. At the same time we can scale the two sets of molecules in two specific orders of activity for pyridyl and amine compounds. For pyridyl compounds the order is 4-pyridyl > 3-pyridyl > 2-pyridyl, both in terms of relative electrophilicity and nucleophilicity, and intermolecular hydrogen bonding is a feasible process. The first amine molecule is a nonperformer, but the second molecule in this series, with a terminal methyl group shows better performance. The molecule with a phenyl ring has the active site located closest to each other, and intramolecular hydrogen bonding does not appear feasible.

HOMO and LUMO of the fluorophore molecules: The HOMO and LUMO of all the receptor ligand molecules were calculated by DFT, and the results are listed in Table 10. All the possible structures were considered, including the non-, mono-, and diprotonated species. The results show that the HOMO—LUMO gap is the smallest in case of diprotonated

Table 10. HOMO and LUMO for all molecules studied.[a]

Molecule[b]	HOMO [eV]	LUMO [eV]
2-phenyl-anth	a) −10.960	a) −8.197
	b) 11.041	b) −8.200
2-pyridyl-anth	a) −10.873	a) −8.189
	b) −11.058	b) −8.205
	c) −11.054	c) −8.206
3-pyridyl-anth	a) −10.919	a) −8.200
	b) −11.049	b) −8.203
	c) −14.511	c) −14.206
4-pyridyl-anth	a) −10.958	a) −8.198
	b) −11.044	b) −8.202
	c) −11.051	c) −8.210
$NH_2CH_2CH_2$-antha[c]	a) −4.627	a) −1.972
	b) −11.051	b) −8.193
	c) −11.045	c) −8.190
$CH_3CH_2NHCH_2$antha[c]	a) −10.852	a) −9.062
	b) −11.400	b) −8.695
	c) −10.224	c) −9.833

[a] a = nonprotonated, b = monoprotonated, c = diprotonated. [b] anth = methylaminomethylanthracene. [c] aminomethylanthracene.

9-*N*-(3-pyridylmethyl)aminomethylanthracene (0.305 eV), and for diprotonated 9-*N*-[2-(methylamino)ethyl]aminomethylanthracene the value is 0.391 eV. For rest of the molecules the difference between HOMO and LUMO is greater than 2 eV. In most cases the HOMO – LUMO gap increases on protonation and decreases for further protonation. This suggests that the electronic transition is more favorable at lower degrees of protonation. That means that for the PET process the transition may occur during the transition from nonprotonated to monoprotonated species, and will be terminated at the diprotonated stage. The transition is favorable in case of 2-, 3-, and 4-pyridyl substituents. This may be due to the particular orientation of the molecule when the nitrogen atom becomes most nucleophilic with a tendency to favorable hydrogen bonding, which is not observed in other cases. The order for neutral molecule is 4-pyridyl – anthracene > 3-pyridyl – anthracene > 2-pyridyl – anthracene > 2-phenyl – anthracene > $NH_2CH_2CH_2$ – anthracene > $CH_3NHCH_2CH_2$ – anthracene. This trend is the same as our predictions from the calculation of reactivity indices for the neutral molecules. This shows that our predictions based on calculation of reactivity indices can successfully be validated by HOMO – LUMO calculations to determine the feasibility of these molecules' acting as fluorophores. For the monoprotonated case the HOMO – LUMO gap folows the order $NH_2CH_2CH_2$ – anthracene > 2-pyridyl – anthracene > 4-pyridyl – anthracene > 3-pyridyl – anthracene > 2-phenyl – anthracene > $CH_3NHCH_2CH_2$ – anthracene. The trend for the diprotonated case is $NH_2CH_2CH_2$ – anthracene > 2-pyridyl – anthracene > 4-pyridyl – anthracene > $CH_3NHCH_2CH_2$ – anthracene > 3-pyridyl – anthracene. From this trend we can state that after monoprotonation, amine-type molecules having the largest band gap cannot act as fluorophores, and the band gap is even wider after diprotonation. It seems that for 3-pyridyl – anthracene the diprotonated species will perform better than the monoprotonated one. These results also show that the active site present in the part associated with a pyridyl ring or amino substituent has a greater contribution to the electronic

transition that closer to the anthracene moiety, the receptor in the system. We now compare the PDOS for the contributing nitrogen centers to determine whether their environment plays a role in their atomic orbital contributions.

Partial density of state calculation for the fluorophore molecules: The PDOS can be used to study the contribution of a particular orbital or group of orbitals to the molecular orbital spectrum. In PDOS, atomic wave functions are projected onto the molecular orbital [Eq. (10)].

$$D_j(E) = \sum_{N}^{i=1} \langle \phi_j \,|\, \psi_i \rangle \delta(E - E_i) n_i \text{[28]} \qquad (10)$$

Thus it gives a reasonable indication of the contribution of the AO ψ_i to the MO ϕ_j, but a major disadvantage is that the values are not normalized. Adding the partial DOS for all orbitals in the system does not give the total number of electrons in the system, because of the nonorthogonality of the basis functions on different atoms. However, qualitative information can still be gathered from the analysis. We used the contribution of the nitrogen atomic orbitals to determine the effect of their environment and to visualize the energy shift occurring due to protonation, which will further help us to propose a plausible mechanism for these fluorophores in the PET process. We determined the PDOS for the nitrogen centers present in the ligands. We first compared the PDOS for the common nitrogen center N25 present in non- and monoprotonated 2-phenyl–anthracene and non-, mono-, and diprotonated species of the other molecules. The results are shown in Figures 7–9. The PDOS of N25 in non- and monoprotonated 9-*N*-(phenylmethyl)aminomethylanthracene are compared in Figure 7. The central peak for

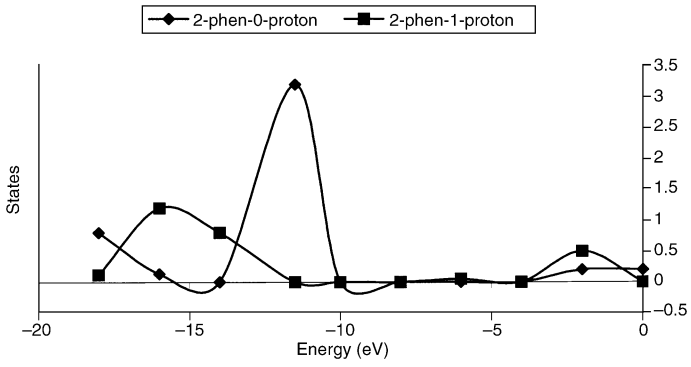

Figure 7. PDOS curve for the N25 center in non- and monoprotonated 9-*N*-(2-phenylmethyl)aminomethylanthracene.

the contributions of p and s orbitals at about −11 eV shifts to lower energy in the protonated form, and thus the probability of fluorescence in the monoprotonated form is decreased. Figure 8 compares the PDOS for the N25 center in the three pyridyl-type molecules. The energy contour for the 3-pyridyl compound is different from those of the other two. The energy difference between the non- and monoprotonated forms is less pronounced than in the other two cases, and the profile moves to a higher energy, so that electron transition in the

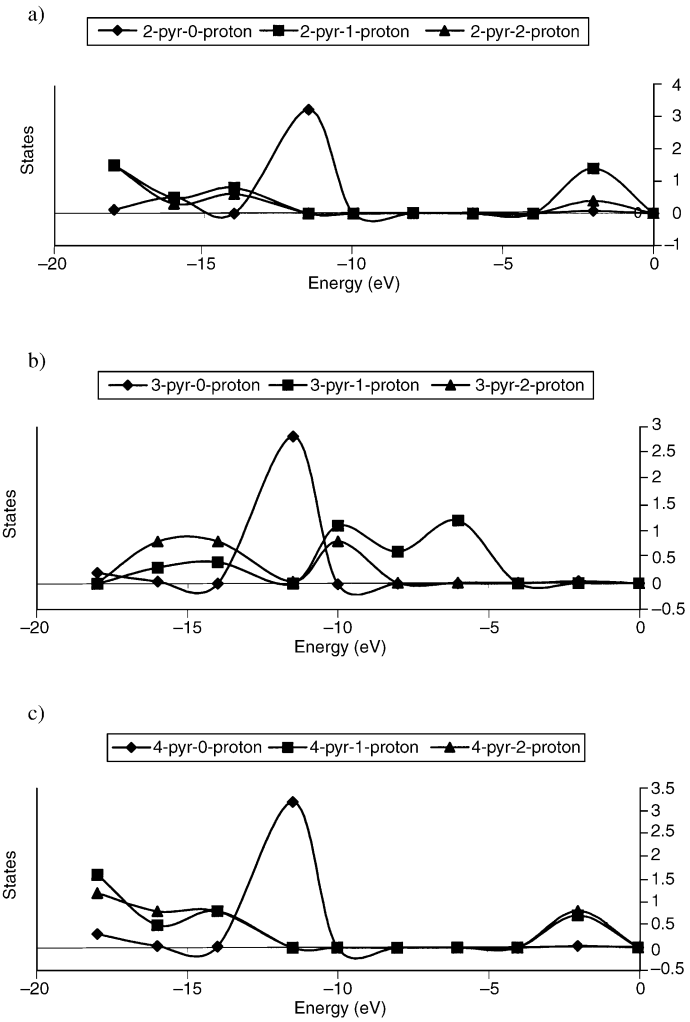

Figure 8. PDOS curve for N25 in non-, mono-, and diprotonated 9-*N*-(2-pyridylmethyl)aminomethylanthracene (a), 9-*N*-(3-pyridylmethyl)aminomethylanthracene (b), and 9-*N*-(4-pyridylmethyl)aminomethylanthracene (c).

monoprotonated is favorable. This also matches well to the trend proposed from the HOMO–LUMO gaps. The comparison of N25 centers for the amine-type compounds in Figure 9 shows different trends for the compounds with $NH_2CH_2CH_2$ and $CH_3NHCH_2CH_2$ substituents. The latter molecule has a higher transition probability in terms of the contour energy difference between the non- and monoprotonated forms. Comparing these data with Figure 8 shows that the central nitrogen atom has different contributions in amine- and pyridyl-type compounds. The PDOS for the pyridyl nitrogen atoms are compared in Figure 10, while the PDOS of N35 of the amine-type molecules are shown in Figure 11. The trends for the pyridyl molecules are similar to those shown in Figure 8, with the exception of the 3-pyridyl compound, for which the contributions for non-, mono-, and diprotonated forms are visually distinct from one another, whereas in other cases they almost overlap with each other. For the amine-type molecules the trend is different from that of Figure 9. The N35 center common to both molecules makes a much larger contribution to the electronic transition than the N25 center. The second molecule of this series will be a better performer

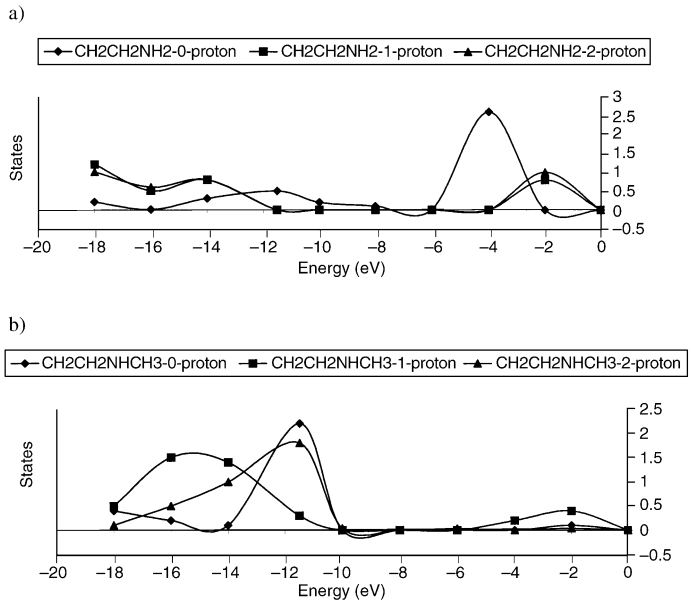

Figure 9. PDOS curve for N38 in a) 9-*N*-(2-aminoethyl)aminomethylanthracene and b) 9-*N*-[2-(methylamino)ethyl]aminomethylanthracene in non-, mono-, and diprotonated forms.

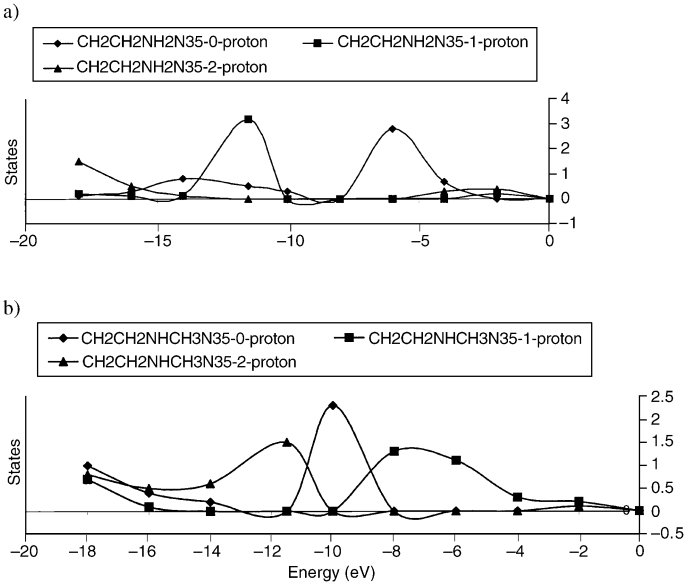

Figure 11. PDOS curve for N35 in a) 9-*N*-(2-aminoethyl)aminomethylanthracene and b) 9-*N*-[2-(methylamino)ethyl]aminomethylanthracene in non-, mono-, and diprotonated forms.

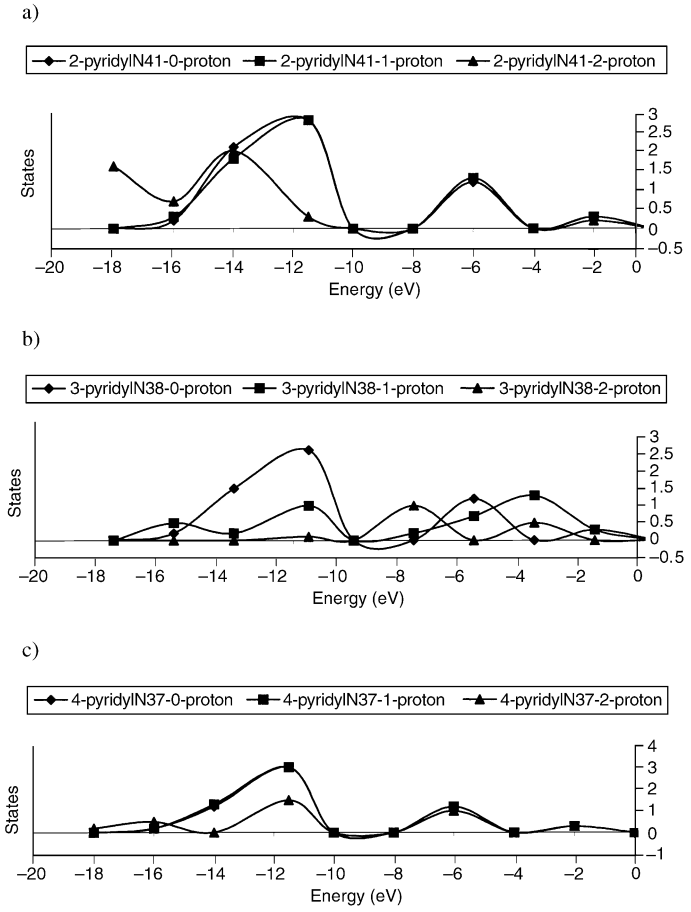

Figure 10. PDOS curve for the pyridyl N atoms in a) 9-*N*-(2-pyridylmethyl)aminomethylanthracene, b) 9-*N*-(3-pyridylmethyl)aminomethylanthracene, and c) 9-*N*-(4-pyridylmethylaminomethylanthracene in non-, mono-, and diprotonated forms.

than the first one. In the case of the other amine compound, the PDOS shows a higher transition probability in terms of the location of the high-intensity contour. The PDOS results show that the atomic contribution from the centers further from the anthracene group have greater contributions than the other centers. This trend also matches the scale of reactivity indices.

Conclusion

This is the first study to rationalize the phenomenon of PET and to select molecules suitable for PET. The aim was to choose the best ligand among a series of molecules. As the PET phenomenon is based on protonation and electronic transition, we predicted that the mechanism can be explained well by the HSAB principle within the domain of DFT. We calculated the local reactivity indices and relative nucleophilicities/electrophilicities to locate the active electrophile and nucleophile in molecules in which a receptor is linked to a fluorophore. This paves the way for visualizing the effect of intramolecular hydrogen bonding between the electrophilic and nucleophilic centers. We compared this behavior for compounds with pyridinyl and aliphatic amino substituents to study the role, location, and configuration of the nitrogen atoms in the process. We also correlated the geometric parameters. This was then followed by the calculation of the HOMO – LUMO band gap of the molecules before and after protonation. We finally plotted the results to show that the 4-pyridyl compound is the best ligand, with small but significant differences in behavior relative to its 2- and 3-pyridyl counterparts. The case of amine-type compounds was also examined. These results were then validated by calculating partial densities of states, which reveal orbital degeneracy. We examined the nitrogen orbital for all cases, and a specific scenario evolved. Since the PET process involves excitation by a photon, which is not the subject of our

study, we investigated the receptor ligands on the basis that if they take part in the PET process they require both nucleophilicity and electrophilicity in the molecule, and the scale of these activities were correlated with their suitability for PET. The HOMO–LUMO gaps and the PDOS show the orbital contributions and describe the degeneracy of electrons. In PET the photon excitation is transmitted through the HOMO–LUMO to end up in a stable state, so the current methodology could be utilized to design receptors according to need. This is the first study on designing fluorescence sensors. The promising results provoked us to perform calculations on the excited states to simulate the fluorescence spectra, and these studies are now underway.

[1] A. P. De Silva, H. Q. N. Gunaratne, T. Gunnlaugsson, A. J. M. Huxley, C. P. McCoy, J. T.Rademacher, T. E. Rice, *Chem. Rev.* **1997**, *97*, 1515.
[2] L.Streyer, *Biochemistry*, 3rd Ed., Freeman, New York, **1988**.
[3] R. Y. Tsien, *Chem. Eng. News* **1994**, July 8, 34.
[4] R. A. Bissel, A. P. De Silva, H. Q. N. Gunaratne, P. L. M. Lynch, G. E. M. Maguire, K. R. A. S. Sandanayake, *Chem. Soc. Rev.* **1992**, *21*, 187.
[5] B. Valeur, "Probe Design and Chemical Sensing", *Top. Fluoresc. Spectrosc.* **1994**, *4*, 21.
[6] A. P. De Silva, H. Q. N. Gunaratne, C. P. McCoy, *Chem. Commun.* **1996**, 2399.
[7] L. Fabbrizi, M. Licchelli, P. Pallavicini, A. Perotti, A. Taglietti, D. Sacchi, *Chem. Eur. J.* **1996**, *2*, 75.
[8] A. P. De Silva, R. A. D. D. Rupasinghe, *Chem. Commun.* **1985**, 1169.
[9] R. G. Pearson, *J. Am. Chem. Soc.* **1983**, *105*, 7512.
[10] R. G. Pearson, *J. Chem. Educ.* **1987**, *64*, 561.
[11] R. G. Parr, W. Yang, *J. Am. Chem. Soc.* **1984**, *106*, 4049.
[12] P. Geerlings, F. De Proft, *Int. J. Quant. Chem.* **2000**, *80*, 227.
[13] L. T. Nguyen, T. N. Le, F. De Proft, A. K. Chandra, W. Langenaeker, M. T. Nguyen, P. Geerlings, *J. Am. Chem. Soc.* **1999**, *121*, 5992
[14] W. Langenaeker, F. D. Proft, P. Geerlings, *J. Phys. Chem. A* **1998**, *102*, 5944.
[15] A. K. Chandra, P. Geerlings, M. T. Nguyen, *J. Org. Chem.* **1997**, *62*, 6419.
[16] A. Chatterjee, T. Iwasaki, T. Ebina, *J. Phys. Chem. A* **1999**, *103*, 2489, and references therein.
[17] A. Chatterjee, T. Iwasaki, *J. Phys. Chem. A* **2001**, *105*, 6187.
[18] A. Chatterjee, T. Iwasaki, T. Ebina, *J. Phys. Chem. A* **2002**, *106*, 641.
[19] R. K. Roy, S. Krishnamurti, P. Geerlings, S Pal, *J. Phys. Chem. A* **1998**, *102*, 3746.
[20] A. Chatterjee, T. Iwasaki, T. Ebina, *J. Phys. Chem. A* **2001**, *105*, 10694.
[21] R. G. Pearson, R. G. Parr, *J. Am. Chem. Soc.* **1983**, *105*, 7512.
[22] W. Yang, M. J. Mortier, *J. Am. Chem. Soc.* **1986**, *108*, 5708.
[23] W. Kohn, L. Sham, *J. Phys. Rev. A* **1965**, *140*, 1133
[24] A. Becke, *J. Chem. Phys.* **1988**, *88*, 2547.
[25] C. Lee, W. Yang, R. G. Parr, *Phys. Rev. B* **1988**, *37*, 786.
[26] C. W. Bock, M. Trachtman, *J. Phys. Chem.* **1994**, *98*, 95.
[27] V. Amendola, L. Fabrizzi, P. Pallavicini, L. Parodi, A. Perotti, *J. Chem. Soc. Dalton Trans.* **1998**, 2053.
[28] Dmol3 User Guide 1999, Molecular Simulations Inc., San Diego, **1999**.

Received: November 26, 2002
Revised: April 15, 2003 [F4613]

